INTERNATIONAL JOURNAL FOR NUMERICAL METHODS IN FLUIDS
Int. J. Numer. Meth. Fluids 2006; **50**:1123–1144
Published online 15 September 2005 in Wiley InterScience (www.interscience.wiley.com). DOI: 10.1002/fld.1071

Multidimensional positive definite advection transport algorithm: An overview

Piotr K. Smolarkiewicz*,†

National Center for Atmospheric Research, Boulder, CO 80307, U.S.A.

SUMMARY

Multidimensional positive definite advection transport algorithm (MPDATA) was proposed in the early eighties as a simple positive-definite advection scheme with small implicit diffusion, for evaluating the advection of water-substance constituents in atmospheric cloud models. Over the two decades, MPDATA evolved from an advection scheme into a class of generalized transport algorithms that expand beyond advective transport to alternate PDEs and complete fluid models with a wide range of underlying governing equations. Recently, MPDATA has attracted attention in the context of several mutually-beneficial developments such as (i) quantification of MPDATA implicit turbulence modelling capability in the spirit of monotonically integrated large eddy simulations (MILES), (ii) extensions to flow solvers cast in generalized time-dependent curvilinear coordinates, and (iii) unstructured-grid formulations. The aim of this paper is to assist the special issue on MPDATA methods for fluids by providing an up to date comprehensive review of the approach, including the underlying concepts, principles of implementation, and guidance to the accumulated literature. Copyright © 2005 John Wiley & Sons, Ltd.

KEY WORDS: nonoscillatory advection schemes; finite volume methods; fluid models

1. INTRODUCTION

The hydrodynamic description of nature is omnipresent from quantum mechanics [1] to astrophysics [2]. The equations describing fluid flows may take a variety of forms, depending upon the physical assumptions involved. However, from the perspective of numerical approximations they may be often reduced to the symbolic form of a generalized transport equation

$$\frac{\partial G\rho\Psi}{\partial t} + \nabla\cdot(G\rho\mathbf{v}\Psi) = G\rho R \tag{1}$$

*Correspondence to: Piotr K. Smolarkiewicz, Mesoscale and Microscale Meteorology Division, National Center for Atmospheric Research, Boulder, CO 80307, U.S.A.
†E-mail: smolar@ucar.edu

Contract/grant sponsor: U.S. Department of Energy

Received 25 March 2005
Revised 2 July 2005
Accepted 17 July 2005

where $G=G(\mathbf{x},t)>0$, $\rho=\rho(\mathbf{x},t)>0$, $\mathbf{v}=\mathbf{v}(\mathbf{x},t)$, and $R=R(\mathbf{x},t)$ are assumed to be known functions of the coordinates. A scalar function G is introduced to admit curvilinearity of the coordinates, so it may play the role of the Jacobian of the coordinate transformation from a physical $(\mathbf{x}_P,t_P)$ to an arbitrary time-dependent curvilinear framework $(\mathbf{x},t)$ [3–5]. Consequently, $\mathbf{v}\equiv\dot{\mathbf{x}}$ should be viewed as the advecting *contravariant* velocity in the $(\mathbf{x},t)$ frame. Because ρ symbolizes a generalized fluid density,[‡] the dependent variable Ψ denotes some fluid property per unit mass (i.e. a mixing-ratio as opposed to a density type variable); e.g. a component of physical velocity (viz. momentum per unit of mass) or specific entropy. On the rhs, R combines all forcings and/or sources. For example, when (1) represents a momentum equation, then R includes the pressure gradient component associated with the velocity component Ψ. In general, both $\mathbf{v}$ and R will be functionals of the dependent variables.

A special case of (1) is $\Psi\equiv 1$ and $R\equiv 0$, for which (1) represents the mass-continuity equation. The latter manipulated with (1) gives an evolution-equation

$$\frac{\mathrm{d}\Psi}{\mathrm{d}t}=R \tag{2}$$

where $\mathrm{d}/\mathrm{d}t\equiv\partial/\partial t+\mathbf{v}\cdot\nabla$. For $R\equiv 0$, the homogeneous equation (2) specifies the invariance of Ψ along flow trajectories. In particular, it conveys that advection alone can change neither the sign nor the extrema of a mixing-ratio variable. Due to the positivity of ρ, the sign preservation property of advection extends to density-type variables; while the preservation of extrema requires solenoidal flows, i.e. $G^{-1}(G_{,t}+\nabla\cdot G\mathbf{v})\equiv 0$. The sign-preservation property is especially important, since, together with the conservation form in (1), it implies that the domain integral of Ψ^2 should remain uniformly bounded for all times, subject to contributions from imposed boundary conditions. These elementary properties of advection underline solutions to complete fluid problems, yet they are difficult to attain using numerical approximations. This is illustrated in Figure 1 that shows the numerical solution to constant-coefficient advection—$\Psi_{,t}+c\Psi_{,x}=0$—on periodic domain, using the classical second-order-accurate centred-in-time-and-space leapfrog scheme. While the analytic solution $\Psi(x,t)=\Psi(x-ct,0)$ merely translates the initial signal,[§] the resulting numerical solution is distorted and oscillatory.

For elementary advection, preserving the extrema or sign of transported variables is somewhat academic, since spurious distortions do not necessarily imply poor overall accuracy. For substantiation, Figure 2 complements the second-order-accurate centered-in-time-and-space solution in Figure 1 with the fourth-order-accurate forward-in-time (viz. time uncentred) scheme of Tremback *et al.* [6], a representative of dissipative Lax–Wendroff (alias Taylor–Galerkin, in the finite-element literature) algorithms. In the numerical simulation of fluids, however, monotone or sign-preserving advection may not be an option, but rather a necessary prerequisite of solution realizability (e.g. for reactive or multi-phase flows). Alas, linear schemes that guarantee smooth solutions having the overall accuracy of second- and higher-order methods do not exist [7]. Consequently, the alternative is either to accept first-order methods with their notorious implicit diffusivity, cf. Figure 3, or to abandon the premise of linearity, and complicate the problem by approximating even the simplest constant-coefficient advection with an elaborate nonlinear scheme.

[‡]For example, if (1) is an archetype of a shallow water system, then ρ will be a local depth of the fluid.

[§]The half-width of a cosine-shaped function is resolved with 12 intervals δx of a uniform grid composed of 500 cells; $c\delta t/\delta x=0.5$, and the solution shown in Figure 1 is after 1600 time steps δt.

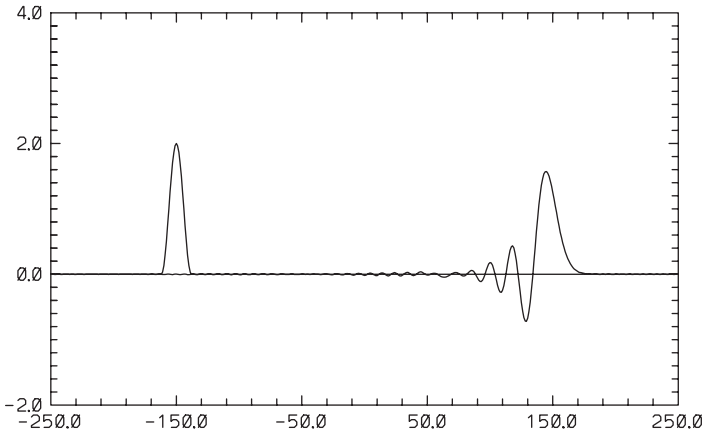

Figure 1. Constant-coefficient numerical advection with the leapfrog scheme. Flow is from left to right, and the solution is downwind of the initial condition.

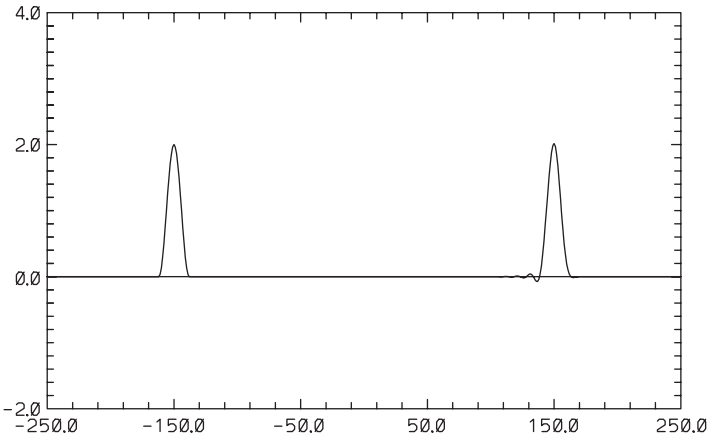

Figure 2. As in Figure 1 but for a fourth-order-accurate Lax–Wendroff scheme.

Multidimensional positive definite advection transport algorithm (MPDATA) [8, 9] is a family of nonlinear finite-volume advection algorithms akin to Lax–Wendroff schemes. Recall that a second-order-accurate one-step Lax–Wendroff scheme can be derived from the first-order-accurate upwind (alias upstream or donor cell) scheme by subtracting from the rhs a space-centred representation of the first-order error. In MPDATA, however, such a compensation is based on a nonlinear estimate of the truncation error, and attained by iterative application of upwind differencing. In the corrective iteration(s) the leading truncation error term (of the upwind scheme) is cast in the form of an advective flux, defined as the product of the current solution iterate and a suitably defined velocity field; see Figure 4, for illustration.

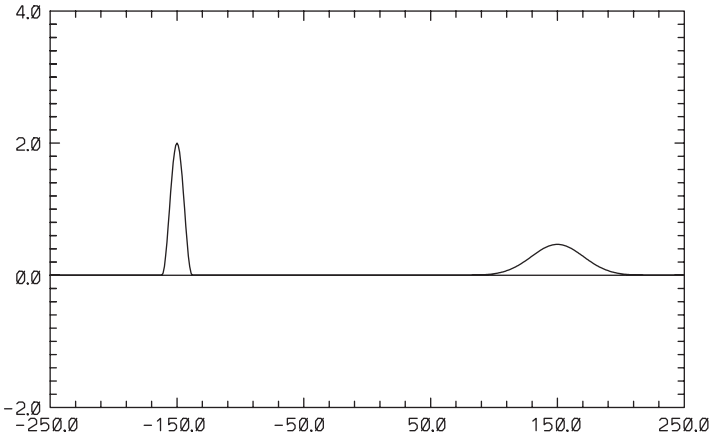

Figure 3. As in Figure 1 but for the first-order-accurate upwind scheme.

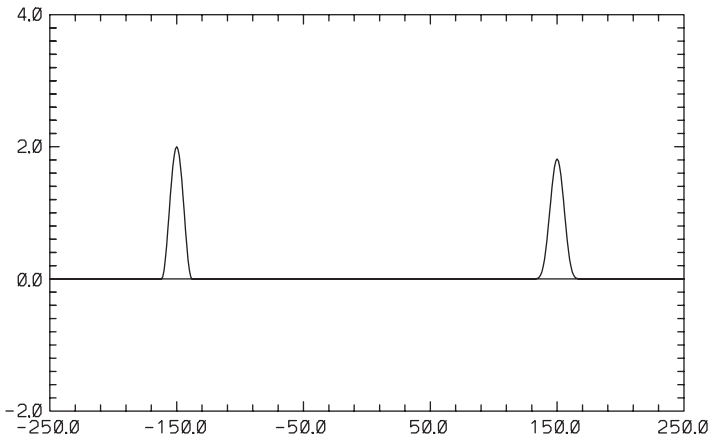

Figure 4. As in Figure 1 but for a second-order-accurate MPDATA scheme.

The theoretical foundation of MPDATA—the modified equation approach—facilitates extending the scheme to the generalized transport problem in (1). Since the origin of MPDATA in the early eighties, a variety of options have been documented that extend MPDATA to curvilinear frameworks, full monotonicity preservation, third-order accuracy, and variable sign fields (such as momentum). MPDATA was generalized to a complete fluid solver in the early nineties [10]. In analysing the truncation error of approximations to (1), one finds error terms that depend on the interaction of advection with the forcing. Many implementations of nonoscillatory algorithms treat advection separately from the forcings, leaving this error uncompensated, thereby reducing the order of accuracy of the solution and potentially leading to oscillations and even instability [11]. In MPDATA, this error is compensated by effectively integrating the forcing terms along a flow trajectory rather than at a grid point.

A comprehensive review of earlier MPDATA developments, including both the underlying concepts and the implementation details, can be found in Reference [12].

Generally speaking, MPDATA belongs to the class of *nonoscillatory* Lax–Wendroff schemes that includes such classical algorithms as FCT [13], TVD [14], and ENO [15]. However, MPDATA is qualitatively different from these other methods, which were developed primarily in the area of high-speed flows to suppress spurious oscillations of Lax–Wendroff schemes for hyperbolic conservation laws. MPDATA was originally developed for meteorological applications—viz. high Reynolds' number, low Mach number flows—to reduce the implicit viscosity of the upwind scheme (commonly used for nonnegative thermodynamic fields in early cloud models) while retaining virtues such as positivity, low phase error, and simplicity of upstream differencing. As a result of its heritage, MPDATA's focus is on sign preserving multidimensional advection rather than on monotone solutions of hyperbolic conservation laws in one spatial dimension. Unlike the TVD and ENO schemes, which employ one-dimensional constructions to limit the scalar flux component, MPDATA effectively limits the magnitude of the vector velocity and so is naturally unsplit. In principle, any of these schemes can be adapted for multidimensional flows of all speeds. However, MPDATA appears to be the first Lax–Wendroff type of approach employed consistently (i.e. for all dependent variables) and successfully throughout a range of fluid models from biomechanics, through geophysics, to solar physics, and involving scales of motion from micro to stellar.

In recent years, a series of studies [16–20] was devoted to quantifying MPDATA's implicit turbulence modelling capability—in the spirit of monotonically integrated large eddy simulations (MILES)—observed in numerous simulations of high Reynolds number flows throughout a range of scales and problems, from breaking of gravity waves in the middle atmosphere to turbulent solar convection [21–25]. Gaining a deeper insight into implicit turbulence modelling is important, as MILES greatly facilitates turbulent-flow studies by obviating the evaluation of the viscous stress—a formidable task in generalized curvilinear frameworks [26]. Unlike most nonoscillatory methods, MPDATA is based directly on the *convexity* of upwind advection[¶] rather than on the idea of flux limiting. The iterative application of upwinding in MPDATA has important physical consequences. In particular, because the upwind scheme filters high frequencies on the grid, and each subsequent step reverses the dissipative error of the preceding step, MPDATA is reminiscent of generalized similarity models, where an estimate of the unfiltered Navier–Stokes velocity (which enters the subgrid-scale stress tensor) is obtained by an approximate inversion of the filtering operation; cf. References [17, 28].

MPDATA has proven successful in simulations of geophysical flows using single block, structured, topologically rectangular meshes, while employing diffeomorphic mappings to accommodate time-dependent curvilinear domains [3, 4, 24, 26]. Its potential for unstructured-grid approximations has been realized only recently. Bacon *et al.* [29] pioneered with an implementation of MPDATA advection in the multiscale environmental model OMEGA for operational forecast of weather and pollutant dispersion. Independently, Margolin and Shashkov [30] drew inspiration from the MPDATA approach to develop a second-order, sign-preserving

[¶]Numerical solutions remain bounded by the surrounding local values of the preceding time step, given a solenoidal advecting flow and an adequately limited time step; for arbitrary flow, the weaker condition of sign preservation can be assured [27].

conservative interpolation for remapping two-dimensional arbitrary Lagrangian–Eulerian (ALE) grids. Aiming at a broad range of applications involving complex, multiply-connected domains and inhomogeneous flows, Smolarkiewicz and Szmelter [27, 31] developed a general, compact edge-based fully unstructured-mesh formulation of MPDATA and extended it to high-speed aerodynamics flows [32].

The goal of this paper is to assist the special issue on the MPDATA methods for fluids that includes a collection of articles devoted to diverse adaptations of the MPDATA approach and its derivatives. With this goal in mind, the remaining part of this paper is organized as follows. The next section summarizes the theoretical foundations of MPDATA schemes in both Cartesian- and unstructured-grid formulations; because the former schemes were reviewed earlier [12], more attention is given to MPDATA for general grids. The computational stability and accuracy of MPDATA are discussed in Section 3. Section 4 reviews extensions of MPDATA important for designing complete fluid models. Theoretical considerations are illustrated with idealized examples, preparing the ground for advanced applications discussed in other papers.

2. BASIC SCHEME

2.1. Cartesian-mesh perspective

In order to convey the key idea underlying the MPDATA approach, it is instructive to assume solenoidal stationary flow, and begin with the 1D flux-form advection equation

$$\frac{\partial \Psi}{\partial t} = -\frac{\partial}{\partial x}(u\Psi) \tag{3}$$

where $u = \text{const}$ is the flow velocity and Ψ a nonnegative scalar field. A general donor-cell approximation to (3) can be written in flux form

$$\Psi_i^{n+1} = \Psi_i^n - [F(\Psi_i^n, \Psi_{i+1}^n, U_{i+1/2}) - F(\Psi_{i-1}^n, \Psi_i^n, U_{i-1/2})] \tag{4}$$

where the flux function F is defined in terms of the local Courant number U by

$$\begin{gathered} F(\Psi_L, \Psi_R, U) \equiv [U]^+ \Psi_L + [U]^- \Psi_R \\ U \equiv \frac{u\delta t}{\delta x}; \quad [U]^+ \equiv 0.5(U + |U|); \quad [U]^- \equiv 0.5(U - |U|) \end{gathered} \tag{5}$$

The integer and half-integer indices correspond to the cell centres and cell walls, respectively, and $[U]^+$ and $[U]^-$ are the nonnegative and nonpositive parts of the Courant number, respectively. A simple truncation error analysis[‖] reveals that the first-order-accurate scheme in (4) approximates, to second-order in δx and δt, the advection–diffusion equation

$$\frac{\partial \Psi}{\partial t} = -\frac{\partial}{\partial x}(u\Psi) - \frac{\partial}{\partial x}\left(-K\frac{\partial \Psi}{\partial x}\right) \tag{6}$$

[‖] All dependent variables are expanded in a Taylor series about a common point, say (x_i, t^n), and all temporal derivatives are expressed in terms of the spatial derivatives using the governing equation.

where

$$K = \frac{(\delta x)^2}{2\delta t}(|U| - U^2) \tag{7}$$

The key idea of MPDATA is to rewrite the Fickian flux in the error term on the rhs of (6) as a convective flux $-K(\partial\Psi/\partial x) \equiv u_d\Psi$, thereby defining the diffusive pseudo velocity

$$u_d \equiv -\frac{(\delta x)^2}{2\delta t}(|U| - U^2)\frac{1}{\Psi}\frac{\partial\Psi}{\partial x} \tag{8}$$

In order to subsequently compensate the first-order error of (4), one again uses the donor-cell scheme but with the *antidiffusive* velocity $\tilde{u} = -u_d$ in lieu of u and with the value of Ψ^{n+1} already updated in (4) *in lieu* of Ψ^n. Choosing a suitable approximation of the ratio $(1/\Psi)(\partial\Psi/\partial x)$ in (8), e.g.

$$\frac{1}{\Psi}\frac{\partial\Psi}{\partial x} \approx \frac{2}{\delta x}\frac{\Psi_{i+1}^{n+1} - \Psi_i^{n+1}}{\Psi_{i+1}^{n+1} + \Psi_i^{n+1} + \varepsilon} \tag{9}$$

assures the stability of the corrective iteration for arbitrary small $\varepsilon > 0$ and $|U| \leqslant 1$.

Extending MPDATA to multiple dimensions is straightforward, except that one needs to account for the cross-derivative terms that appear in the truncation error of the donor-cell scheme. For example, in 2D the elementary advection equation (3) becomes

$$\frac{\partial\Psi}{\partial t} = -\frac{\partial}{\partial x}(u\Psi) - \frac{\partial}{\partial y}(v\Psi) \tag{10}$$

and its donor-cell approximation

$$\begin{aligned}\Psi_{i,j}^{n+1} = \Psi_{i,j}^n &- [F(\Psi_{i,j}^n, \Psi_{i+1,j}^n, U_{i+1/2,j}) - F(\Psi_{i-1,j}^n, \Psi_{i,j}^n, U_{i-1/2,j})] \\ &- [F(\Psi_{i,j}^n, \Psi_{i,j+1}^n, V_{i,j+1/2}) - F(\Psi_{i,j-1}^n, \Psi_{i,j}^n, V_{i,j-1/2})]\end{aligned} \tag{11}$$

where now U and V are the dimensionless Courant numbers

$$U \equiv \frac{u\delta t}{\delta x} \quad \text{and} \quad V \equiv \frac{v\delta t}{\delta y} \tag{12}$$

and the flux function F has been defined in (5). Note that in contrast to 1D, solenoidal flow does not imply uniform velocity. The truncation error analysis reveals that (11) approximates to second-order the advection–diffusion equation

$$\begin{aligned}\frac{\partial\Psi}{\partial t} = &-\frac{\partial}{\partial x}(u\Psi) - \frac{\partial}{\partial y}(v\Psi) \\ &+ \frac{(\delta x)^2}{2\delta t}(|U| - U^2)\frac{\partial^2\Psi}{\partial x^2} + \frac{(\delta y)^2}{2\delta t}(|V| - V^2)\frac{\partial^2\Psi}{\partial y^2} - \frac{UV\delta x\delta y}{\delta t}\frac{\partial^2\Psi}{\partial x\partial y}\end{aligned} \tag{13}$$

As in 1D, the diffusive fluxes are cast in convective form, thereby defining antidiffusive pseudo velocities in the x and y directions; e.g.

$$\begin{aligned}\widetilde{u} &= \frac{(\delta x)^2}{2\delta t}(|U| - U^2)\frac{1}{\Psi}\frac{\partial \Psi}{\partial x} - \frac{UV\delta x\delta y}{2\delta t}\frac{1}{\Psi}\frac{\partial \Psi}{\partial y} \\ \widetilde{v} &= \frac{(\delta y)^2}{2\delta t}(|V| - V^2)\frac{1}{\Psi}\frac{\partial \Psi}{\partial y} - \frac{UV\delta x\delta y}{2\delta t}\frac{1}{\Psi}\frac{\partial \Psi}{\partial x}\end{aligned} \tag{14}$$

By selecting uniformly bounded approximations to the ratios $(1/\Psi)\nabla\Psi$, one assures the stability of the corrective iteration.

2.2. *Unstructured-grid formulation*

In an arbitrary finite-volume framework, formal derivation of MPDATA [27, 31] is somewhat more difficult than for Cartesian meshes. For example, distinguishing between single and multiple dimensions or assuming constant velocity loses its instructional appeal, since unstructured grid dictates anisotropy and inhomogeneity of local Courant numbers even for uniform flows. In spite of increased mathematical complexity, the unstructured-grid formalism is more compact, while more general. In particular, we consider now a Euclidean advection problem

$$\frac{\partial \Psi}{\partial t} = -\nabla\cdot(\mathbf{v}\Psi) \tag{15}$$

where $\mathbf{v}$ is an arbitrary stationary flow, and Ψ at $t = 0$ is assumed nonnegative.

To aid in explaining the notation, Figure 5 shows a face of an arbitrary computational cell containing vertex i, together with the *edge* connecting vertex i with one of its immediate neighbours j; there are $l(i)$ edges connecting the vertex i with its neighbours. S_j refers both to the face *per se* and to its surface area. Integrating (15) over the cell volume (while employing the Gauss divergence theorem) results in

$$\Psi_i^{n+1} = \Psi_i^n - \frac{\delta t}{\mathcal{V}_i}\sum_{j=1}^{l(i)} F_j^{\perp} S_j \tag{16}$$

This is exact, given Ψ_i^{n+1} and Ψ_i^n are interpreted as the mean values of Ψ within the volume $\mathcal{V}_i$ of the cell containing vertex i, while $F_j^{\perp}$ is interpreted as the mean normal flux through the

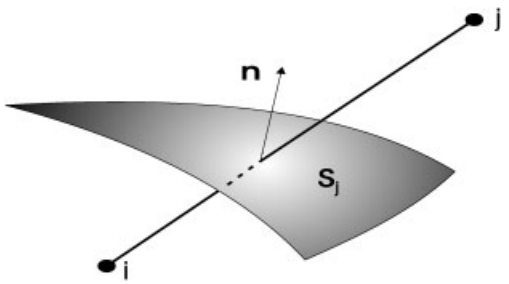

Figure 5. Schematic of an edge piercing a face of an arbitrary 3D cell.

cell face S_j averaged over temporal increment δt. The approximation begins with specifying fluxes $F_j^{\perp}$ in terms of data available on the grid. Analogous to the Cartesian donor-cell scheme (4)–(5), an arbitrary-grid finite-volume upwind assumes

$$F_j^{\perp} = [v_j^{\perp}]^{+}\Psi_i^n + [v_j^{\perp}]^{-}\Psi_j^n \tag{17}$$

where normal velocity $v^{\perp} \equiv \mathbf{v}\cdot\mathbf{n}$ is evaluated at the face S_j. The nonnegative/nonpositive parts of $v_j^{\perp}$ always coincide with outflow/inflow from the ith cell.

The leading truncation error of the unstructured-grid upwind differencing is determined by expanding all discrete data into a Taylor series in time and space, about the intermediate time $t^{n+1/2}$ and point s_j where the edge pierces the face, and then representing higher-order temporal derivatives in terms of spatial derivatives [27, 31]. In effect, the upwind flux in (17) becomes decomposed into a time-centred flux through the face and a first-order truncation-error flux of a predominantly Fickian character

$$\begin{aligned} F_j^{\perp} &= v_j^{\perp}\Psi|_{s_j}^{n+1/2} + \text{Error} \\ \text{Error} &= -0.5|v_j^{\perp}|\left.\frac{\partial\Psi}{\partial r}\right|_{s_j}^{*}(r_j - r_i) + 0.5v_j^{\perp}\left.\frac{\partial\Psi}{\partial r}\right|_{s_j}^{*}(r_i - 2r_{s_j} + r_j) \\ &\quad + 0.5\delta t v_j^{\perp}(\mathbf{v}\nabla\Psi)|_{s_j}^{*} + 0.5\delta t v_j^{\perp}(\Psi\nabla\cdot\mathbf{v})|_{s_j}^{*} + \mathcal{O}(\delta r^2, \delta t^2, \delta t\delta r) \end{aligned} \tag{18}$$

where r refers to the parametric description of the edge $r(\lambda) = r_i + \lambda(r_j - r_i)$; $\lambda \in [0,1]$, and the asterisk superscripts in Error symbolize either time level n, $n+1/2$, or $n+1$, as any of these can be considered without affecting the form or the order of Error.

As with Cartesian meshes, unstructured-grid MPDATA consists of a sequence of upwind (16)–(17) iterations. In the first iteration, the input field and flow velocity, Ψ and $\mathbf{v}$, are taken from the preceding time step t^n. In the second (corrective) iteration, the input field Ψ is the result of the preceding upwind iteration and the pseudo velocity $\tilde{v} := -(1/\Psi)\text{Error}$. In particular,

$$\begin{aligned} \tilde{v}_j^{\perp} &= 0.5|v_j^{\perp}|\left(\frac{1}{\Psi}\frac{\partial\Psi}{\partial r}\right)\Bigg|_{s_j}^{*}(r_j - r_i) - 0.5v_j^{\perp}\left(\frac{1}{\Psi}\frac{\partial\Psi}{\partial r}\right)\Bigg|_{s_j}^{*}(r_i - 2r_{s_j} + r_j) \\ &\quad - 0.5\delta t v_j^{\perp}\left(\mathbf{v}\frac{1}{\Psi}\nabla\Psi\right)\Bigg|_{s_j}^{*} - 0.5\delta t v_j^{\perp}(\nabla\cdot\mathbf{v})|_{s_j}^{*} \end{aligned} \tag{19}$$

with the asterisk now indicating the first-order estimate of the $n+1$ solution from the preceding upwind iteration. In principle, the entire process of estimating the residual error and the associated compensation can be continued, iteration after iteration, reducing the magnitude of the truncation error—reducing the formal order of the error requires third-order analysis to begin with, cf. Reference [33]—yet in practice one corrective iteration suffices for recovering the overall accuracy of time-space centred schemes.

The procedure outlined above conveys the essence of the arbitrary-grid finite-volume MPDATA in abstraction from any specific data distribution and details of the discrete

representation of differential operators. Although derived for edges, the general form of the pseudo velocity (19) applies to many finite volume schemes with various cell arrangements. In particular, (19) indicates that some specifications of control volumes may be optimal for MPDATA because they simplify the leading truncation error of the upwind scheme and reduce the computational effort associated with evaluating the anti-truncation-error pseudo velocity. In particular, the median-dual finite-volume approach (see Reference [34] for a comprehensive discussion) constructs the control volume associated with the vertex i by joining the centres of polyhedra cells and midpoints of the edges surrounding the vertex i, Figure 6; thereby cancelling out the mesh skewness error in the second term on the rhs of (19).

Having defined the mesh, all geometric elements such as cell volumes, cell face areas, and normals are evaluated from elementary vector calculus. Hereafter, $\mathbf{S}_j \equiv S_j \mathbf{n}_j$ symbolizes the oriented surface element with $\mathbf{n}_j$ denoting the normal. Because normal fluxes in (16) are always proportional to normal velocities $\mathbf{v}_j \cdot \mathbf{n}_j$, the face surface area $S_j = \| \mathbf{S}_j \|$ can be conveniently incorporated in the definition of the normal velocity $v_j^{\perp} := \mathbf{v}_j \cdot \mathbf{S}_j$ while setting $S_j \equiv 1$ in all relevant formulae. Consequently, the surface-area-weighted advective velocities normal to the cell face S_j are evaluated at cell faces as

$$v_j^{\perp} = \mathbf{S}_j \cdot 0.5[\mathbf{v}_i + \mathbf{v}_j] \tag{20}$$

whereupon the surface-weighted antidiffusive pseudo velocity can be approximated as

$$\hat{v}_j^{\perp} = |v_j^{\perp}| \frac{\Psi_j^* - \Psi_i^*}{\Psi_j^* + \Psi_i^* + \varepsilon} - \frac{\delta t}{2} v_j^{\perp} \left(\mathbf{v} \cdot \frac{\nabla \Psi^*}{\overline{\Psi^*}} + \nabla \cdot \mathbf{v} \right)_{S_j} \tag{21}$$

where Ψ^* denotes the result after the generic upwind iteration, and ε is a small constant, e.g. 10^{-10}, assuring that the denominator does not vanish when $\Psi_j^* = \Psi_i^* = 0$. The factor in brackets on the rhs of (21) is written symbolically for conciseness. Because the complete technical exposition is elaborate and given in Reference [27], here we only comment on its two principal aspects. First, $\overline{\Psi^*}$ denotes the arithmetic average of Ψ^*s taken from the grid points employed for evaluating $\nabla \Psi^*$, thereby exploiting the elementary boundedness property $|\sum \pm \Psi / \sum \Psi| \leqslant 1$ of positive-definite scalar fields, important for MPDATA stability. Second, following Reference [29], the weighted convective derivative $\sim \mathbf{v} \cdot (\nabla \Psi^* / \overline{\Psi^*})$ is evaluated entirely in terms of Cartesian components. This departs from the Cartesian-grid MPDATA in

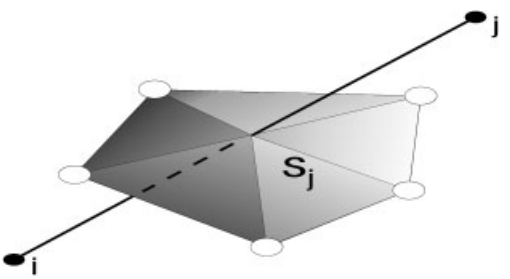

Figure 6. The edge-based median-dual approach. The edge connecting vertices i and j pierces the face S_j of a 3D computational cell surrounding vertex i. Open circles represent centres of polyhydra cells referred to in the text.

Section 2.1, where, due to the mesh orthogonality, the 'diagonal' elements of $v_j^{\perp}\mathbf{v}\cdot(\nabla\Psi^*/\overline{\Psi^*})$ were combined into $\sim(|U|-U^2)$ and $\sim(|V|-V^2)$ terms in (14). In a general finite-volume framework, the latter would require an additional effort associated with decomposing the complete convective derivative into derivatives normal and tangential to cell faces. While it is unnecessary for standard MPDATA schemes with a single corrective iteration, such a development may become essential for multiple upwind passes or higher-order options; cf. Reference [33] for additional insights.

3. ACCURACY, STABILITY, AND BENCHMARK RESULTS

The basic MPDATA schemes described in Sections 2.1 and 2.2 are constructed from the classical upwind scheme, which is consistent, conditionally stable, and first-order accurate. These properties, together with the algorithm's design, predetermine the consistency, stability, and accuracy of MPDATA [9]. In particular, because the pseudo velocities (8), (14), or (19) tend to zero as the spatial and temporal increments decrease, the consistency of MPDATA is implied by that of upwind. Similarly, because the corrective upwind iteration compensates the first-order leading error of the preceding upwind step, with accuracy at least to first-order, the uncompensated portion of the upwind error remains at second-order. The latter suffices to increase the formal accuracy order of upwinding on a Cartesian-mesh—second- and third-order asymptotic convergence rates of various MPDATA options have been documented for Cartesian meshes, cf. Reference [12] and references therein. For arbitrary meshes, however, this is not necessarily the case, since the formal accuracy of the centred scheme—a target of the MPDATA derivation, in (18)—is not mesh independent [35]. Notwithstanding, Bacon *et al.* [29] demonstrated second-order convergence of their cell-centred unstructured MPDATA using a standard 'rotating-cone' benchmark while invoking intensive local mesh refinement. Furthermore, Smolarkiewicz and Szmelter [27] have shown second-order accuracy for their edge-based formulation on both quality and skewed unstructured median-dual grids; see also Reference [36] in the same issue for an illustration and further discussion.

The stability of MPDATA also follows that of the upwind scheme, but there is a subtlety. Following Reference [27], we note first that

$$\forall_i \sum_{j=1}^{l(i)} [U_j]^+ \leqslant 1; \quad U_j := \frac{v_j^{\perp} S_j \delta t}{\mathscr{V}_i} \tag{22}$$

suffices for the upwind advection in (16)–(17) to preserve the nonnegative/nonpositive character of the transported fields, thereby amounting to satisfaction of the nonlinear stability condition; cf. Reference [16] for a discussion. For solenoidal flows, (22) suffices for solution convexity, and reduces to

$$\sum_{j=1}^{l(i)} |U_j| \leqslant 2 \tag{23}$$

a stability condition familiar from the finite-difference literature, e.g. (4) in Reference [9]. Stability proofs for MPDATA rely on showing that, for each corrective iteration, local Courant

numbers are bounded by the local Courant numbers of the preceding iteration. In one spatial dimension, (21) together with the stability and positivity of the original upwind scheme implies

$$|\hat{U}_j| \leqslant |U_j| - (U_j)^2 \leqslant |U_j| \tag{24}$$

so that the stability of upwind ensures the stability of MPDATA. A similar result occurs in multidimensional problems, but the presence of cross-derivatives makes a formal proof difficult. In Reference [9], it has been proven that the stability of upwind assures the stability of the Cartesian-mesh MPDATA, but with the caveat that the time step used is smaller than that allowed for the upwind alone by the factor $2^{-1/2}$ and 2^{-1}, in 2 and 3 spatial dimensions, respectively. This particular time step requirement follows from assuming a worst case scenario where the velocity components flip sign across the cell. Because the latter is a rare event in CFD applications, the heuristic limit recommended for all structured-mesh MPDATA extensions has been the same as that for the upwind scheme. A similar result has been argued and verified for the unstructured-mesh formulation [27].

We illustrate the performance of basic MPDATA using a standard solid-body rotation test [8, 9, 12]. A cone of base radius 15 and height 4, centred initially at $(75, 50)$, is rotating counter-clockwise around the centre of a $[0, 100] \times [0, 100]$ domain with angular velocity $\omega = 0.1$. Figure 7 displays the isolines of the exact result and of two MPDATA solutions after 6 rotations. These results were generated with the edge-based unstructured-grid formulation of MPDATA [27, 31]. The solution in the central plate uses 10^4 square cells, whereas the solution in the right plate uses a triangular grid with a similar number and distribution of points. For reference, all parameters of the test and of the display are identical to those in Figure 1 in Reference [12], which showed similar results generated with the Cartesian-mesh formulation of MPDATA. The solution using square cells is indistinguishable from the corresponding result in Figure 1 of Reference [12]—a demonstration of the generality and reflexivity of the unstructured grid formulation. The accuracy of the results displayed is quantified in Table I, where the corresponding values for the classical upwind and centred-in-time-and-space leapfrog schemes are included for the sake of reference.

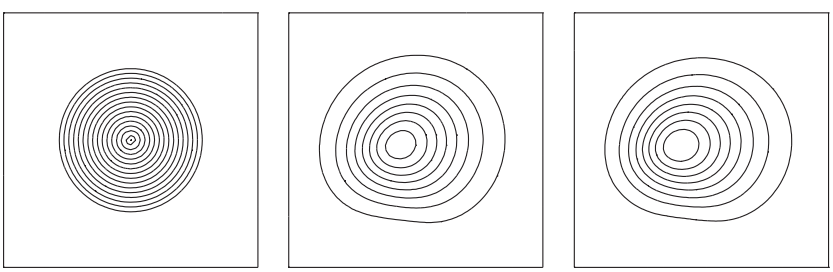

Figure 7. Isolines of a cone advected through six rotations around the centre of the lower frame (only a quarter of the domain is shown). The contour interval is 0.25, and the zero contour line is not shown. Left plate, the analytic solution; centre plate, the finite-volume MPDATA on a regular square-mesh; right plate, as in the centre but for a triangular mesh.

Table I. Error norms for solid-body rotation test using Cartesian and unstructured grid formulations of MPDATA; the classical upwind and centred-in-time-and-space leapfrog schemes are included.

Scheme	Formulation (grid)	Max	Min	L_2
MPDATA	Cartesian	2.18	0.00	0.47×10^{-3}
MPDATA	Unstructured (squares)	2.18	0.00	0.47×10^{-3}
MPDATA	Unstructured (triangles)	2.19	0.00	0.47×10^{-3}
upwind	Cartesian	0.27	0.00	1.21×10^{-3}
upwind	Unstructured (squares)	0.28	0.00	1.04×10^{-3}
upwind	Unstructured (triangles)	0.25	0.00	1.06×10^{-3}
Leapfrog	Cartesian	3.16	−0.62	0.62×10^{-3}
Leapfrog	Unstructured (squares)	3.11	−0.67	0.64×10^{-3}
Leapfrog	Unstructured (triangles)	3.11	−0.69	0.65×10^{-3}

4. EXTENSIONS TO FLOW SOLVERS

The basic MPDATA scheme can be supplemented by numerous extensions that either enhance the accuracy and generality of the MPDATA advection, or expand its capabilities beyond advective transport to alternate PDEs and to complete flow solvers; cf. Reference [12] for a review. Here, we summarize a few selected extensions that are of particular importance for many applications, and are routinely employed in flow simulations discussed in other papers collected in the special issue.

4.1. Generalized transport equation

It is instructive to discuss selected MPDATA options in terms of the reduced generalized transport equation (1)

$$\frac{\partial G\Psi}{\partial t} + \nabla \cdot (\mathbf{v}\Psi) = GR \tag{25}$$

where the density ρ has been absorbed either in G, or in Ψ and R. The latter distinction depends on the elastic versus inelastic character of the governing fluid equations,** and determines the interpretation of Ψ as a density or mixing-ratio type variable. This freedom of interpretation benefits the efficacy of Taylor-series based flow solvers such as MPDATA. For example, in inelastic systems it suffices to cancel truncation errors depending on the flow divergence, regardless of the complexity of the accompanying mass continuity equation [24]; whereas in elastic systems it assures consistency of advective transport for all dependent variables [11]. Depending upon the definition of G, $\mathbf{v} \equiv G\dot{\mathbf{x}}$ should be viewed as either a generalized 'advective' velocity or a momentum vector.

In order to design a fully second-order MPDATA flow solver, it is important to derive the leading truncation error terms for (25) rather than to hastily combine the basic scheme with,

**The terms elastic and inelastic are used to distinguish between a compressible versus an incompressible character of the PDE used to describe the flow. For example, consider the shallow water equations—a long-wave approximation for incompressible stratified flows—that are mathematically akin to the compressible-flow Euler equations.

e.g. a time-centred representation of the rhs forcing. Such derivations [12, 24] reveal terms that depend on the interaction of the advection with the forcing, and on the coordinate transformation as well as on the time dependence of the flow. Because these terms are rooted in the uncentred time-discretization, they are independent of the spatial discretization, whereupon all related developments (cf. References [12, 24] for a discussion) are common to structured- and unstructured-grid frameworks. For example, discretizing (25) in time as

$$\frac{G^{n+1}\Psi^{n+1} - G^n\Psi^n}{\delta t} + \nabla\cdot(\mathbf{v}^{n+1/2}\Psi^n) = (GR)^{n+1/2} \tag{26}$$

leads to the modified equation

$$\frac{\partial G\Psi}{\partial t} + \nabla\cdot(\mathbf{v}\Psi) = GR - \nabla\cdot\left[\frac{\delta t}{2}G^{-1}\mathbf{v}(\mathbf{v}\cdot\nabla\Psi) + \frac{\delta t}{2}G^{-1}\left(\frac{\partial G}{\partial t} + \nabla\cdot\mathbf{v}\right)\mathbf{v}\Psi\right]$$
$$+\nabla\cdot\left(\frac{\delta t}{2}\mathbf{v}R\right) + \mathcal{O}(\delta t^2) \tag{27}$$

Specifying the time levels of both the advective velocity and the forcing term as $n+1/2$ in (26) eliminates $\mathcal{O}(\delta t)$ truncation errors proportional to their temporal derivatives [12]. Although any $\mathcal{O}(\delta t^2)$ approximations to $\mathbf{v}^{n+1/2}$ and $R^{n+1/2}$ will suffice for compensating these error terms, the preference depends on the elastic vs inelastic character of the governing system. For example, in inelastic systems a linearly extrapolated $\mathbf{v}^{n+1/2}$ readily satisfies the mass continuity equation; whereas in elastic systems, a nonlinear extrapolation consistent with the governing equations of motion (viz. predictor) admits larger δt [11].

The second term on the rhs of (27) is a generalization of the quadratic (in velocity) error terms that appear throughout (7), (13) and (18); its compensation is within the realm of the basic MPDATA, cf. (8), (14) and (19). Its second component is multiplicative of the flow divergence in elastic systems, and multiplicative of the mass continuity equation in inelastic systems; both accounting for the possible time dependence of curvilinear coordinates. Because mass continuity in numerical models is satisfied to (at least) the truncation error, this second component is conveniently negligible in inelastic systems; e.g. facilitating dynamic mesh adaptivity. While a similarly convenient temporal discretization is conceivable for the elastic case, to our knowledge, it has not been accomplished yet with MPDATA.

The term on the rhs of (27) proportional to the convective flux of R couples the advection and forcing. Many implementations of nonoscillatory algorithms treat advection separately from the forcings, relying on experience with centred-in-time-and-space methods. However, leaving this error uncompensated not only reduces the order of accuracy of the solution but also amplifies oscillations and can even lead to instability [11]. To illustrate, we slightly modify the constant-coefficient advection example from the introduction. Consider a system composed of two advection equations coupled by restoring forces

$$\Psi_{,t} + c\Psi_{,x} = \omega\Phi; \qquad \Phi_{,t} + c\Phi_{,x} = -\omega\Psi \tag{28}$$

with $\Phi = 0$ at $t = 0$. This is a minimalistic model of a harmonic oscillator that translates with velocity c and transforms Ψ in Φ, and *vice versa*, with frequency $\omega = 2\pi/(400\delta t)$, Figure 8.

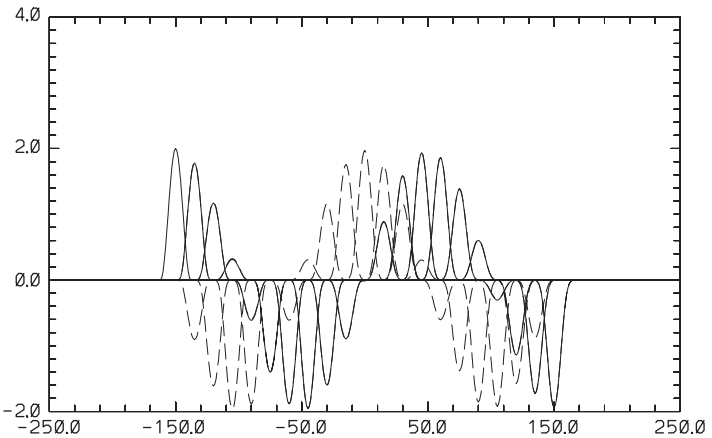

Figure 8. Solution sequence over $t = 600\delta t$, for Ψ (solid line) and Φ (dashed line) dependent variables of the translating oscillator in (28); otherwise as in Figure 4.

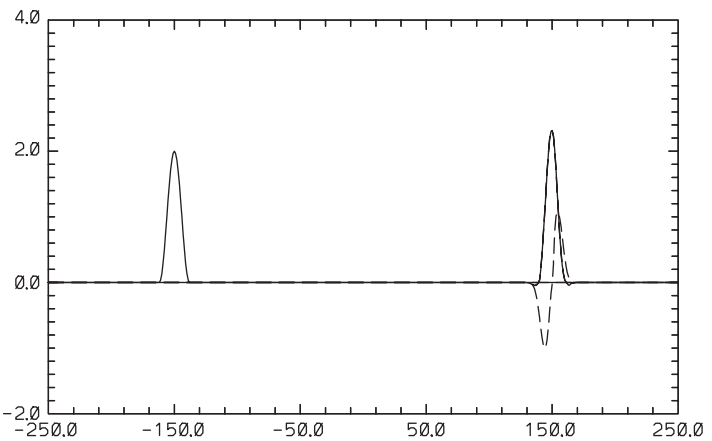

Figure 9. As in Figure 4 but for the translating oscillator in (28), evaluated with (29).

A naive integral of (28) can be compactly written as

$$\Psi_i^{n+1} = \Psi_i^* + \delta t\omega 0.5(\Phi_i^n + \Phi_i^{n+1}), \quad \Phi_i^{n+1} = \Phi_i^* - \delta t\omega 0.5(\Psi_i^n + \Psi_i^{n+1}) \tag{29}$$

where $(.)_i^* \equiv \mathscr{M}_i(., c)$ symbolizes the output from a homogeneous advection MPDATA module. Figure 9 displays the solution—implied in the implicit algebraic system (29)—after $t = 1600\delta t$, as in Figure 4. While the analytic solution requires repetition of the initial shape, numerical results exhibit spurious decoupling of the two components. Despite the second-order advection and the trapezoidal integral of the rhs, the solution still suffers from first-order error proportional to the convective flux of the rhs. A trivial (programming-wise) alteration of the

algorithm in (29)

$$\Psi_i^{n+1} = \Psi_i^* + \delta t\omega 0.5\Phi_i^{n+1}, \quad \Phi_i^{n+1} = \Phi_i^* - \delta t\omega 0.5\Psi_i^{n+1} \tag{30}$$

with $\Psi_i^* \equiv \mathscr{M}_i(\Psi^n + \delta t\omega 0.5\Phi^n, c)$ and $\Phi_i^* \equiv \mathscr{M}_i(\Phi^n - \delta t\omega 0.5\Psi^n, c)$—a paraphrase of the Strang splitting [37]—has a profound impact on the quality of the result. It effectively compensates the coupling error, producing a solution indistinguishable from that in Figure 4.†† This is because at each grid point

$$\mathscr{M}(\Psi^n + \delta t\omega 0.5\Phi^n, c) = \Psi^n + \delta t\omega 0.5\Phi^n - \delta t\overline{c\Psi_{,x}} - \delta t\overline{c(\delta t\omega 0.5\Phi)_{,x}} + \text{HOT} \tag{31}$$

where $\overline{(.)}$ symbolizes the integral over δt, and HOT denotes higher order terms. The second term on the rhs of (31) combines with the second term on the rhs of the first equation in (30) to give the trapezoidal integral of the forcing, and the fourth term is the negative of the coupling error term, with accuracy up to the higher order terms. An analogous argument holds for Φ.

In a time–space continuum, advection may be interpreted as a remapping of the transported field $\Psi(\mathbf{x}, t)$ to the feet $(\mathbf{x}_o(\mathbf{x}, t),\ t_o)$ of flow trajectories arriving at $(\mathbf{x}, t)$ points of the continuum. Consequently, advecting in (30) the field plus half of the forcing ($\times \delta t$) amounts to integrating the rhs of the equations along flow trajectories—consistent with the Lagrangian form (2) of the generalized transport problem—using the trapezoidal rule; see Reference [11] and references therein, for further discussion. Extending (30) to the more general form (25) results in

$$\Psi_i^{n+1} = \frac{G_i^n}{G_i^{n+1}}\mathscr{M}_i(\Psi^n + 0.5\delta tR^n,\ \mathbf{v}^{n+1/2},\ G^n) + 0.5\delta tR_i^{n+1} \tag{32}$$

the principal algorithm of the high-performance 3D program EULAG‡‡ for simulating rotating, stratified flows in complex geometries, on scales from micro to planetary [24]. The only two extensions of the basic MPDATA required for (32) are: (i) the G^{-1} factors in the antidiffusive velocity terms indicated in (27); and (ii) a generalized form of the antidiffusive velocity permitting the advection of fields of variable sign such as momenta. The approach adopted in (30) and (32) for compensating the $\sim \delta t\nabla\cdot(\mathbf{v}R)$ error term in (27) is effective for a broad range of fluid models, but by no means exclusive; for discussion and other options see References [11, 12] and references therein.

4.2. *Transporting fields of variable sign*

Until now, we have assumed that the transported field Ψ is exclusively either nonnegative or nonpositive—in fact, only $\Psi \geqslant 0$ was addressed, but all formulae hold for $\Psi \leqslant 0$, given $\varepsilon < 0$ in (9) and (21). This assumption is important for stability, accuracy, and in general, for the design of MPDATA. However, it enters MPDATA schemes explicitly only in the pseudo velocity formulae, in the $\sim \Delta\Psi/\sum\Psi$ terms of the discrete approximations to the components of $\sim \Psi^{-1}\nabla\Psi$ ratios—cf. (8), (14), and (19). These terms are bounded when Ψ is of constant

†† Indeed, the algorithm in (30) has been employed to produce the solution sequence in Figure 8.

‡‡ The name EULAG [22] alludes to the capability to solve the inelastic fluid equations in either an Eulerian (flux form [11]) or a Lagrangian (advective form [38]) framework.

sign, but can lead to arbitrarily large pseudo velocities and unstable schemes when Ψ changes sign. MPDATA can be extended to the transport of variable-sign fields in several ways. Below we outline two extensions that have proven useful in applications.

The simplest and most common way is to replace all Ψs in (8), (14), and (19) with $|\Psi|$s; exploiting the relationship[§§]

$$\frac{1}{\Psi}\frac{\partial \Psi}{\partial x} \equiv \frac{1}{2\mu}\frac{1}{(\Psi^2)^\mu}\frac{\partial (\Psi^2)^\mu}{\partial x}\bigg|_{\mu=1/2} = \frac{1}{|\Psi|}\frac{\partial |\Psi|}{\partial x} \tag{33}$$

The results are, for all practical purposes, insensitive to the value of μ; however, $\mu = 1/2$ is the optimal choice as it only requires replacing Ψ with $|\Psi|$ in the pseudo velocity formulae derived for the constant-sign fields and is, furthermore, computationally the most efficient. This approach has been employed in the translating-oscillator example in the preceding subsection.

An alternate approach exploits the mass continuity equation (Section 4 in Reference [39]). Multiplying (25)—with $\Psi \equiv \chi$ being the fluid density (elastic systems), or with $\Psi \equiv \chi \equiv 1$ and a steady reference density included in G (inelastic systems)—by an arbitrary constant c and adding the resulting equation to (25) leads to

$$\frac{\partial G(\Psi + c\chi)}{\partial t} + \nabla \cdot (\mathbf{v}(\Psi + c\chi)) = GR \tag{34}$$

which illustrates yet another degree of freedom in MPDATA. The arbitrary constant c can be chosen to assure positivity of Ψ^n, while making MPDATA susceptible to asymptotic linear analysis as $c \nearrow \infty$, [39]. Furthermore, MPDATA itself can be linearized about an arbitrarily large constant leading to a two-pass scheme that differs technically from the basic algorithm in only two details: at the second iteration, the donor cell flux function in (5) or (17) takes the value unity in its two Ψ-arguments, and the pseudo velocities in (8), (14) and (19) replace each Ψ with unity in all '$\sum \Psi$' denominators. This asymptotic form of MPDATA—often referred to as the 'infinite gauge'—is a realization of the classical Lax–Wendroff algorithm (cf. Section 4 in Reference [39]). For advection of constant-sign fields it gives solutions attainable with basic MPDATA, except that it is not sign preserving; Figure 10. However, since it preserves the solution slope at zero crossings, it has been a preferred option for transporting momenta in fluid models, especially when combined with monotonicity enhancement [12, 16, 18–20].

4.3. Nonoscillatory option

The basic MPDATA scheme described in Section 2 preserves the sign but not the monotonicity of the transported variables [9, 39, 40] and, in general, the solutions are not free of spurious extrema, Figure 11. This is because the antidiffusive velocity is not necessarily solenoidal, even for a solenoidal physical flow. In many studies of natural flows, the preservation of sign is adequate. However, when required, MPDATA can be made fully monotone [40] by adapting the flux-corrected-transport (FCT) formalism [13] to limit the pseudo velocities; cf.

[§§]For a discussion of some formal issues at $\Psi \to 0$ see Section 3.2 in Reference [39].

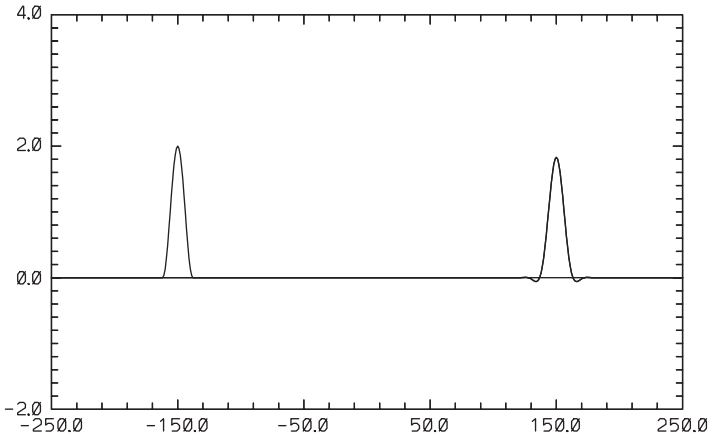

Figure 10. As in Figure 4 but for the 'infinite-gauge' option of MPDATA.

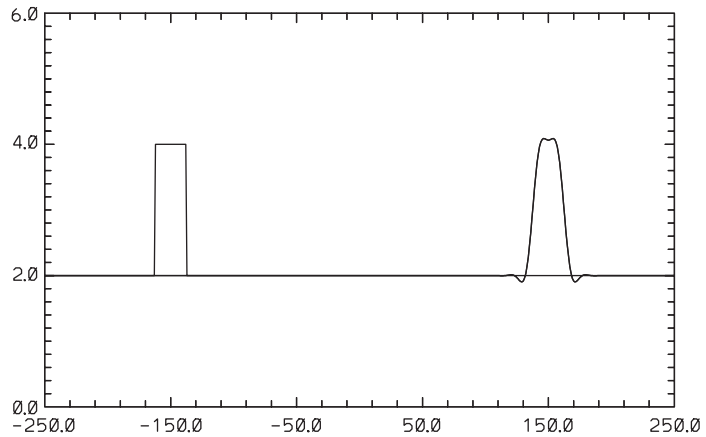

Figure 11. As in Figure 4 but for a rectangular signal on constant background.

Figure 12. It can be argued [40] that MPDATA is particularly well suited for this adaptation for several reasons. Firstly, the initial MPDATA iteration is the upwind scheme—a low-order monotone scheme commonly used as the reference in the FCT design. Secondly, assuring monotonicity of the subsequent iterations provides a higher-order accurate reference solution for the next iteration with the effect of improving the overall accuracy of the resulting FCT scheme. Thirdly, because all MPDATA iterations have similar low phase errors characteristic of the upwind scheme [39], the FCT procedure mixes solutions with consistent phase errors. This benefits the overall accuracy of the resulting FCT scheme (see Figure 5 in Reference [40] and the accompanying discussion).

The FCT extension for the Cartesian-mesh MPDATA was presented in Reference [40] together with an algebraic theory of FCT limiting—the algebraic formalism has proven

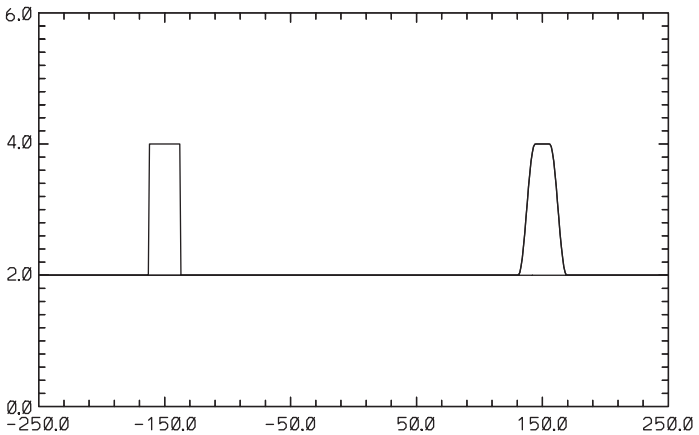

Figure 12. As in Figure 11, but for the nonoscillatory-option MPDATA solution.

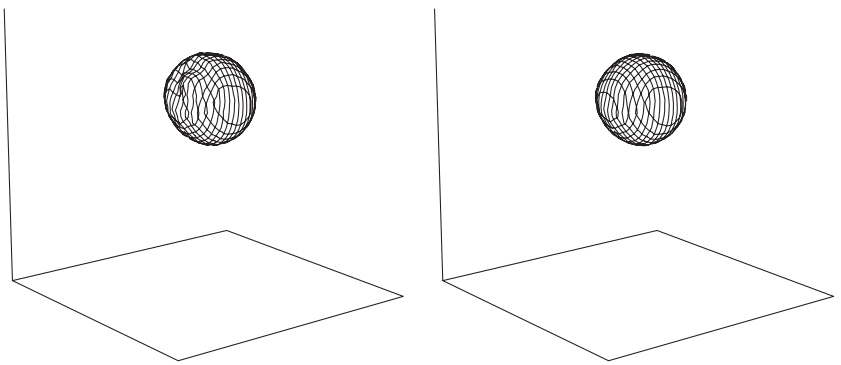

Figure 13. Leapfrog-trapezoidal-FCT (left), and infinite-gage-FCT MPDATA (right) solutions after one revolution of the sphere on unstructured grid.

useful for synchronous FCT where physical bounds imposed on functions of transported fields alter the standard limiters of the individual fields [41, 42]. Recently, a technical summary of the relevant formulae and details of the implementation as well as 3D benchmark calculations were presented in Reference [27], in the context of the edge-based unstructured-grid algorithm; Figure 13 shows two of their solutions. The test case adopted is an extension of the solid-body rotation problem from Section 3 to three spatial dimensions: A sphere with radius 15 and constant density 4, placed initially at $\mathbf{x}_o = (25,\ 75,\ 75)$, rotates with angular velocity $\boldsymbol{\omega} = 0.1 \times 3^{-1/2}(1,\ 1,\ 1)$ around a diagonal of the cuboidal domain $[0,\ 100] \times [0,\ 100] \times [0,\ 100]$. The two solutions displayed in the left and right plates are, respectively, for the FCT leapfrog-trapezoidal scheme [13] and the infinite-gauge-FCT MPDATA. The solutions use an unstructured grid with background spacing 2, roughly a twice coarser resolution than that employed in the 2D examples discussed earlier. Both solutions are evaluated after $T = 10 \times 2\pi \approx 556\delta t$, i.e. after one revolution of the sphere around the

domain diagonal. While both solutions are free of spurious oscillations, statistics of the solution errors reveal the superior accuracy of the MPDATA result [27]; e.g. the better symmetry of the MPDATA solution is evident in Figure 13.

5. CONCLUDING REMARKS

The intent of this overview of MPDATA was twofold. First, it was aimed at setting the background for a series of technical papers collected in the special issue, by providing a self-contained summary of the theoretical foundations of the approach and a guide to the MPDATA literature. Second, it was intended to draw the reader's attention to essential impediments one may need to account for, when taking a journey from an elementary constant-coefficient advection to complete hydrodynamic models.

The body of literature devoted to advection schemes is enormous. In the neverending quest for the perfect advection scheme, the broader perspective—that fluid models are superior structures whose overall accuracy may depend critically on their weakest link—often becomes forgotten. As the importance of balancing model errors is gaining increased attention in the computational literature, cf. References [43–46], it may be worth pointing out that the philosophy of MPDATA development has been an aggregation of nonlinear stability, associated with sign-preserving control-volume advection, and second-order accuracy in all aspects of fluid models.

Over the last two decades, MPDATA has been frequently compared with other transport schemes, primarily in the context of passive scalar advection. The assessments of MPDATA's relative strengths and weaknesses reported in the literature depend very much on the schemes included in comparisons, choice of test problems, MPDATA's options, and details of the implementation. The most common critiques are that the basic MPDATA is too diffusive, while enhanced MPDATAs are too expensive. The most often acknowledged virtues are MPDATA's multidimensionality, robustness, and its underlying conceptual simplicity. These advantages carry over to complete fluid models, where the relative efficiency of advection becomes less important with the increasing complexity of other model physics.

In general, nonoscillatory advection algorithms are much more expensive computationally than linear schemes [27], and preserving the monotonicity or sign of transported variables is clearly not cost effective for pure advection. In the numerical simulation of fluids, however, monotone or sign-preserving advection is often not an option but a necessary prerequisite of solution realizability, cf. References [21, 41, 47]. Furthermore, the relatively high cost of nonoscillatory advection, does not necessarily imply a more expensive fluid model. Consider, for example, the benefits of MILES for studies of complex turbulent flows by circumventing the evaluation of viscous stresses [48], or the accelerated convergence of elliptic solvers due to a better conditioning of the rhs [49].

The advancement of MPDATA spans over two decades, but is by no means complete. Recent developments in the areas of implicit turbulence modelling [17, 19, 20], dynamic grid deformation via continuous mappings [3, 50], and unstructured-grid formulations [27, 29, 30] call for further research. Moreover, the outstanding issue of synchronized limiting [41, 42] still awaits general solution for an arbitrary fluid problem.

ACKNOWLEDGEMENTS

Personal reviews by Robert Sharman and Stephen Thomas are gratefully acknowledged. This work was supported in part by the U.S. Department of Energy 'Climate Change Prediction Program' (CCPP) research initiative.

REFERENCES

1. Bialynicki-Birula I, Cieplak M, Kaminski J. *Theory of Quanta*. Oxford University Press: New York, 1992.
2. Sofue Y, Fujimoto M, Wielebinski R. Global structure of magnetic fields in spiral galaxies. *Annual Review of Astronomy and Astrophysics* 1986; **24**:459–497.
3. Prusa JM, Smolarkiewicz PK. An all-scale anelastic model for geophysical flows: dynamic grid deformation. *Journal of Computational Physics* 2003; **190**:601–622.
4. Wedi NP, Smolarkiewicz PK. Extending Gal-Chen and Somerville terrain-following coordinate transformation on time dependent curvilinear boundaries. *Journal of Computational Physics* 2004; **193**:1–20.
5. Prusa JM, Gutowski WJ. MPDATA and grid adaptivity in geophysical fluid flow models. *International Journal for Numerical Methods in Fluids* 2005; *ibid.*
6. Tremback CJ, Powell J, Cotton WR, Pielke RA. The forward-in-time upstream advection scheme: extension to higher orders. *Monthly Weather Review* 1987; **115**:540–555.
7. Godunov SK. A difference scheme for numerical computation of discontinuous solutions of equations in fluid dynamics. *Matematicheskij Sbornik* 1959; **47**:271–306.
8. Smolarkiewicz PK. A simple positive definite advection scheme with small implicit diffusion. *Monthly Weather Review* 1983; **111**:479–486.
9. Smolarkiewicz PK. A fully multidimensional positive definite advection transport algorithm with small implicit diffusion. *Journal of Computational Physics* 1984; **54**:325–362.
10. Smolarkiewicz PK. On forward-in-time differencing for fluids. *Monthly Weather Review* 1991; **119**:2505–2510.
11. Smolarkiewicz PK, Margolin LG. On forward-in-time differencing for fluids: extension to a curvilinear framework. *Monthly Weather Review* 1993; **121**:1847–1859.
12. Smolarkiewicz PK, Margolin LG. MPDATA: a finite-difference solver for geophysical flows. *Journal of Computational Physics* 1998; **140**:459–480.
13. Zalesak ST. Fully multidimensional flux-corrected transport algorithms for fluids. *Journal of Computational Physics* 1979; **31**:335–362.
14. Sweby PK. High resolution schemes using flux limiters for hyperbolic conservation laws. *SIAM Journal on Numerical Analysis* 1984; **21**:995–1011.
15. Harten A, Engquist B, Osher S, Chakravarthy SR. Uniformly high-order accurate essentially non-oscillatory schemes III. *Journal of Computational Physics* 1987; **71**:231–303.
16. Smolarkiewicz PK, Prusa JM. VLES modeling of geophysical fluids with nonoscillatory forward-in-time schemes. *International Journal for Numerical Methods in Fluids* 2002; **39**:799–819.
17. Margolin LG, Rider WJ. A rationale for implicit turbulence modeling. *International Journal for Numerical Methods in Fluids* 2002; **39**:821–841.
18. Margolin LG, Smolarkiewicz PK, Wyszogrodzki AA. Implicit turbulence modeling for high Reynolds number flows. *Journal of Fluids Engineering* 2002; **124**:862–867.
19. Domaradzki JA, Xiao Z, Smolarkiewicz PK. Effective eddy viscosities in implicit large eddy simulations of turbulent flows. *Physics of Fluids* 2003; **15**:3890–3893.
20. Domaradzki JA, Radhakrishnan S. Effective eddy viscosities in implicit modeling of decaying high Reynolds number turbulence with and without rotation. *Fluid Dynamics Research* 2005; **36**:385–406.
21. Prusa JM, Smolarkiewicz PK, Garcia RR. On the propagation and breaking at high altitudes of gravity waves excited by tropospheric forcing. *Journal of the Atmospheric Sciences* 1996; **53**:2186–2216.
22. Smolarkiewicz PK, Margolin LG. On forward-in-time differencing for fluids: an Eulerian/semi-Lagrangian nonhydrostatic model for stratified flows. *Atmosphere-Ocean Special* 1997; **35**:127–152.
23. Margolin LG, Smolarkiewicz PK, Sorbjan Z. Large-eddy simulations of convective boundary layers using nonoscillatory differencing. *Physica D* 1999; **133**:390–397.
24. Smolarkiewicz PK, Prusa JM. Forward-in-time differencing for fluids: simulation of geophysical turbulence. In *Turbulent Flow Computation*, Drikakis D, Guertz BJ (eds). Kluwer Academic Publishers: Dordrecht, 2002; 279–312.
25. Elliott JR, Smolarkiewicz PK. Eddy resolving simulations of turbulent solar convection. *International Journal for Numerical Methods in Fluids* 2002; **39**:855–864.
26. Smolarkiewicz PK, Prusa JM. Towards mesh adaptivity for geophysical turbulence. *International Journal for Numerical Methods in Fluids* 2005; **47**:789–801.
27. Smolarkiewicz PK, Szmelter J. MPDATA: an edge-based unstructured-grid formulation. *Journal of Computational Physics* 2005; **206**:624–649.

28. Domaradzki JA, Adams NA. Direct modelling of subgrid scales of turbulence in large eddy simulation. *Journal of Turbulence* 2002; **3**:1–19.
29. Bacon DP *et al.* A dynamically adapting weather and dispersion model: the operational environment model with grid adaptivity (OMEGA). *Monthly Weather Review* 2000; **128**:2044–2076.
30. Margolin LG, Shashkov M. Second-order sign-preserving conservative interpolation (remapping) on general grids. *Journal of Computational Physics* 2003; **184**:266–298.
31. Smolarkiewicz PK, Szmelter J. Multidimensional positive definite advection transport algorithm (MPDATA): an edge-based unstructured-data formulation. *International Journal for Numerical Methods in Fluids* 2005; **47**:1369–1374.
32. Szmelter J, Smolarkiewicz PK. A low-implicit-diffusion flow solver for unstructured meshes. *AIAA 2005-0321 Paper*.
33. Margolin LG, Smolarkiewicz PK. Antidiffusive velocities for multipass donor cell advection. *SIAM Journal on Scientific Computing* 1998; **20**(3):907–929.
34. Barth TJ. Aspects of unstructured grids and finite volume solvers for the Euler and Navier–Stokes equations. *Special Course on Unstructured Grid Methods for Advection Dominated Flows*, *AGARD. Report 787*, 1992; 6.1–6.61.
35. Roe PL. Error estimates for cell-vertex solutions of the compressible Euler equations. *ICASE Report No. 87-6* 1987; 40.
36. Szmelter J, Smolarkiewicz PK. MPDATA error estimator for mesh adaptivity. *International Journal for Numerical Methods in Fluids* 2005; *ibid.*
37. Strang G. On the construction and comparison of difference schemes. *SIAM Journal on Numerical Analysis* 1968; **5**:506–517.
38. Smolarkiewicz PK, Pudykiewicz JA. A class of semi-Lagrangian approximations for fluids. *Journal of the Atmospheric Sciences* 1992; **49**:2082–2096.
39. Smolarkiewicz PK, Clark TL. The multidimensional positive definite advection transport algorithm: further development and applications. *Journal of Computational Physics* 1986; **67**:396–438.
40. Smolarkiewicz PK, Grabowski WW. The multidimensional positive definite advection transport algorithm: nonoscillatory option. *Journal of Computational Physics* 1990; **86**:355–375.
41. Grabowski WW, Smolarkiewicz PK. Monotone finite-difference approximations to the advection-condensation problem. *Monthly Weather Review* 1990; **118**:2082–2097.
42. Schär C, Smolarkiewicz PK. A synchronous and iterative flux-correction formalism for coupled transport equations. *Journal of Computational Physics* 1996; **128**:101–120.
43. Knoll DA, Chacon L, Margolin LG, Mousseau VA. On balancing approximations for time integration of multiple time scale systems. *Journal of Computational Physics* 2003; **185**:583–611.
44. Klemp JB, Skamarock WC, Fuhrer O. Numerical consistency of metric terms in terrain-following coordinates. *Monthly Weather Review* 2003; **131**:1229–1239.
45. Grabowski WW, Smolarkiewicz PK. A multiscale anelastic model for meteorological research. *Monthly Weather Review* 2002; **130**:939–956.
46. Jauberteau F, Dubois T, Temam R, Tribbia J. Multilevel schemes for the shallow water equations. *Journal of Computational Physics* 2005; **207**:660–694.
47. Margolin LG, Reisner JM, Smolarkiewicz PK. Application of the volume of fluid method to the advection-condensation problem. *Monthly Weather Review* 1997; **125**:2265–2273.
48. Smolarkiewicz PK, Margolin LG, Wyszogrodzki AA. A class of nonhydrostatic global models. *Journal of the Atmospheric Sciences* 2001; **58**:349–364.
49. Smolarkiewicz PK, Grubišić V, Margolin LG. On forward-in-time differencing for fluids: stopping criteria for iterative solutions of anelastic pressure equations. *Monthly Weather Review* 1997; **125**:647–654.
50. Iselin JP, Prusa JM, Gutowski WJ. Dynamic grid adaptation using the MPDATA scheme. *Monthly Weather Review* 2002; **130**:1026–1039.

